ORIGINAL PAPER

Multiscale modeling of solid stress and tumor cell invasion in response to dynamic mechanical microenvironment

H. Chen[1,2] · Y. Cai[1] · Q. Chen[1] · Z. Li[1,2]

Abstract

Mathematical models can provide a quantitatively sophisticated description of tumor cell (TC) behaviors under mechanical microenvironment and help us better understand the role of specific biophysical factors based on their influences on the TC behaviors. To this end, we propose an off-lattice cell-based multiscale mathematical model to describe the dynamic growth-induced solid stress during tumor progression and investigate the influence of the mechanical microenvironment on TC invasion. At the cellular level, cell–cell and cell–matrix interactive forces depend on the mechanical properties of the cells and the cancer-associated fibroblasts in the stroma, respectively. The constitutive relationship between the interactive forces and cell migrations obeys the Hooke's law and damping effects. At the tissue level, the integrated growth-induced forces caused by proliferating cells within the simulation region are balanced by the external forces applied by the surrounding host tissues. Then, the cell movements are calculated according to the Newton's second law of motion, and the morphology of TC invasion is updated. The simulation results reveal the continuous changes of the macroscopic mechanical forces due to the interactions among the structural components and the microscopic environmental factors. Moreover, the simulation results demonstrate the adverse effect of the stiffness of tumor tissue on tumor growth and invasion. A decrease in the stiffness of tumor and matrix can promote TCs to proliferate at a much faster rate and invade into the surrounding healthy tissue more easily, whereas an increase in the stiffness can lead to an aggressive morphology of tumor invasion. We envision that the proposed model can be served as a quantitative theoretical platform to study the underlying biophysical role of the mechanical microenvironmental factors during tumor invasion and metastasis.

Keywords Multiscale model · Solid stress · Early tumor progression · Mechanical microenvironment

1 Introduction

As one of the most important characteristics of tumor microenvironment, solid stress generated by the rapid proliferation of cancer cells is accumulated within tumors during tumor progression. The solid stress can be classified into two types (Jain et al. 2014; Jeroen et al. 2006; Triantafyllos et al. 2012). One is known as cell proliferation-induced stress or residual stress, which includes the microscopic interactions among the structural components (such as stroma, tumor cell and host tissue) in the tumor microenvironment, and it remains in the tumor after external loads are removed (Triantafyllos et al. 2012, 2013). The other is understood as the externally applied stress, which is generated by the neighboring host tissue to inhibit tumor expansion, and it diminishes after tumor excision (Cheng et al. 2011; Demou 2010; Kaufman et al. 2005).

So far, a large amount of experimental data have revealed the influences of solid stresses on tumor pathophysiology, including the direct compression on tumor and stromal cells (Cheng et al. 2011; Helmlinger et al. 1997; Paszek and Weaver 2004; Pierre-Jean et al. 2009; Tse et al. 2012) and indirect deformation of blood and lymphatic vessels (Baish

---

✉ Z. Li
   zhiyong.li@qut.edu.au

1 School of Biological Science and Medical Engineering, Southeast University, Nanjing 210096, China

2 School of Chemistry, Physics and Mechanical Engineering, Queensland University of Technology, Brisbane, QLD 4001, Australia

et al. 2011; Huang et al. 2013; Jain 2013; Kamoun et al. 2010; Pries et al. 2010). In fact, the interactions between tumors and their surrounding mechanical microenvironment involve phenomena in multiple scales. For example, at the cellular level, cancer-associated fibroblasts (CAFs) in stroma are activated during tumor progression and subsequently become desmoplastic, which increases tissue stiffness (Branton and Kopp 1999; Ishihara et al. 2017; Pankova et al. 2016). The stretch on collagen by tumor cells and CAFs, and cell–extracellular matrix (ECM) interactions during migrations of tumor and stromal cells yield the growth-induced stress (Butcher et al. 2009). While at the tissue level, the growth-induced stress is restricted by the surrounding host tissue, which allows the tumor expansion and invade by deforming the surrounding tissue. Advances in experimental and theoretical studies of these multiscale mechanisms are needed to gain more insight into the underexposed role of the mechanical environmental factors in tumor progression and therapy.

Although several in vitro experiments are able to mimic the solid stress induced at different stages of tumor growth (Cheng et al. 2011; Kalli and Stylianopoulos 2018; Montel et al. 2012; Triantafyllos et al. 2013), little is known about the in vivo dynamic mechanical microenvironment. One reason is that currently there are no high-resolution real-time methods to quantify the solid stresses in in vitro or in vivo tumors. Although atomic force microscopy (AFM) has been widely used to image and characterize the mechanical properties of tumor in situ, such as stiffness of tumor cells, measuring and mapping the solid stress induced by tumor growth have proven to be very challenging due to both the heterogeneity of tumor tissue and the presence of residual stresses in tumors. Recently, Jain's group developed and compared three ex vivo and in situ experimental methods (Nia et al. 2017), including the planar cut method, the slicing method and the needle biopsy method, to quantify the stress-induced deformation by high-resolution ultrasonography or optical microscopy. The solid stress was then estimated using mechanical modeling based on Hooke's law. However, the stiffness heterogeneities of the tumor tissue were not fully considered in their model.

Extensive mathematical and computational models of growth-induced solid stress in tumors have been established in recent years, which have facilitated the understanding of tumor cell responses to mechanical microenvironment (Ambrosi and Mollica 2002; Ambrosi and Preziosi 2009; MacLaurin et al. 2012; Triantafyllos et al. 2012, 2013). Recent studies investigated the correlation between the tumor cells proliferation and surrounding tissues by combining biochemical and biomechanical factors (Xue et al. 2016, 2017; Yin et al. 2019). Mathematical modeling of the mechanical microenvironment in tumors can be classified into continuum model and discrete model based on

different modeling methodologies (Jeon et al. 2010; Yazdi et al. 2016). Continuum models treat tumors as isotropic hyper-elastic materials (Chen et al. 2014; Kyriacou et al. 1999; Voutouri et al. 2014) or poroelastic materials (Fraldi and Carotenuto 2018; Islam et al. 2018; Netti et al. 1995; Yin et al. 2019) and contain relatively small number of parameters (Roose et al. 2003), so that they can be simulated efficiently. However, these models are limited in the truth that tumors are not isotropic, and their structures are too complex to be described by a global constitutive equation. In addition, the individual cell properties and the cell–cell and cell–matrix interactions cannot be included in the continuum model. To couple the dynamic microenvironment that the tumor cells experience with their different phenotypes in metastasis, discrete models including agent-based models (Drasdo and Hohme 2005; Smirnov et al. 2010; Zhang et al. 2007) and cellular automaton models (Hatzikirou et al. 2010; Mallet and De Pillis 2006; Patel et al. 2001) have been developed. Following a discrete approach, the tumor cells are represented by one or several agents, while the cell–cell interactions are rule-based according to the local microenvironment. The main drawback of discrete modeling is the limitation of the number of individual cells due to the huge computational cost for simulation. Therefore, hybrid discrete–continuum models of tumor migration and invasion have been proposed (Anderson 2005; Jeon et al. 2010; Stolarska et al. 2009), in which the dynamics of chemicals (such as oxygen, ECM and growth factors) can be solved by using reaction–diffusion–convection partial differential equations (PDEs). Additional ordinary differential equations (ODEs) can also be coupled to describe signaling or metabolic pathways, which can improve the hybrid model to cover multiscale pathophysiological phenomenon.

In this study, we proposed an off-lattice cell-based multiscale mathematical model to quantitatively describe the dynamic growth-induced solid stress during the early tumor progression and investigated the effect of the mechanical microenvironmental factors on the tumor invasion. It is worth mentioning that the stage of the early tumor progression is avascular (Mueller-Klieser 1987; Ribeiro et al. 2017). The model consists of three components in tumor microenvironment, including tumor cells (TCs), host cells (HCs) and ECM. At the cellular level, the interaction forces between the cells depend on the cell mechanical properties, such as stiffness and damping ratio, while forces between the cells and stroma are related to the CAF mechanical properties in the ECM. At the tissue level, the force applied on the cells within a simulated region is balanced by an applied external force from the surrounding host tissue. After that, the cell migration is calculated on the basis of the Newton's second law of motion, and the invasive morphology of tumor is updated. Extensive simulations by adjusting the mechanical parameters of the cell and the surrounding host tissue

are performed in order to assess the influence of different mechanical microenvironments on the tumor invasion.

2 Materials and methods

The present model shown in Fig. 1 consists of three fundamental components within the tumor microenvironment, i.e., TCs, HCs and ECM. The fundamental modeling method used here is distinct element method (DEM), which is based upon the assumption that one particle element only interacts with its neighboring contact elements under a small time step. Therefore, the force acting on the particle element and the element's displacement are determined by its interaction with the neighboring contact elements. In detail, the force and displacement are iteratively calculated by applying defined force–displacement constitutive relationship of interelement contacts and Newton's second law of motion. The constitutive relationship is composed of linear-elastic and viscoelastic contacts, and the two types of contact forces are determined by the relative movement between the element and its neighboring contact element. Newton's second law of motion is used to determine the motion of the element according to the calculated resultant forces on it. The three components (TCs, HCs and ECM) are all assumed to be deformable disks, and each component disk has a set of parameters describing its attributes including size, stiffness, damping coefficient, etc. A detailed description of

their parameters is provided in Supporting Material [S1]. Here, the stiffnesses of the two types of cells and the ECM are simplified to be constants. Moreover, the discrete ECM with an initial number density (the radius of ECM particle is 1 μm and the corresponding ECM number density is 0.712 Unit/μm^2) is uniformly distributed in a simulated region. In addition, we also assumed that the cell–cell adhesions (TC–TC, TC–HC and HC–HC) during separation of two cells are induced by the cancer-associated fibroblasts (CAFs) in the ECM, which resist the cell separation. Thus, the variable mechanical properties of the CAFs result in different bonding effects on the cell–cell adhesions.

The multiscale model is established based on the fact that due to the tumor invasion, the solid stress (or the microscopic interactions between the three components) inside the simulated region is increased, and correspondingly, the applied external stress from the surrounding host tissue at the expanding boundary is also increased. At the cellular level, the cell migration is expressed by the Newton's second law of motion, and the cell–cell interaction is modeled by the Kelvin–Voigt viscoelastic law. At the tissue level, the tumor invasion is described by the whole solid stress field within the simulated region. Considering the balance between the solid stress and the applied external stress at the expanding boundary, the multiscale model is numerically solved by the DEM. The mathematical model and numerical implementation are described in detail in the following sections and Supporting Material [S2].

Fig. 1 Illustration of the multiscale model. The green square represents a simulated region; the blue, red, and purple disks represent the TCs, the HCs, and the ECM, respectively. Black arrows indicate the interactions between the three fundamental components at the cellular level. The yellow arrows represent the forces of the three components acting on the wall, which are balanced by the applied external forces from the surrounding host tissue at the tissue level
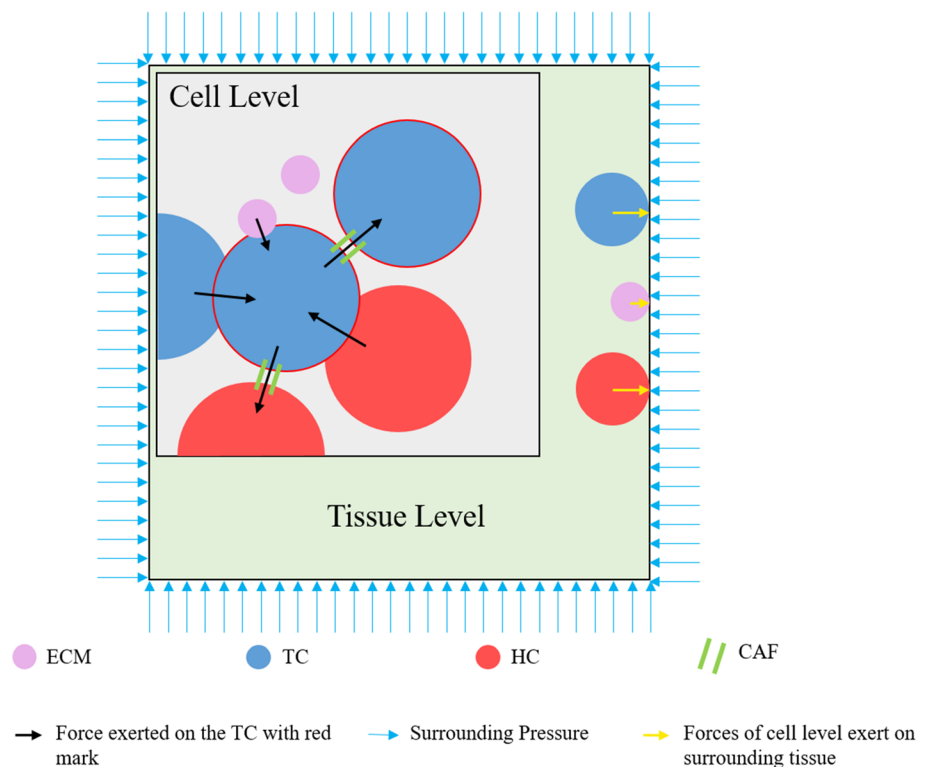
2.1 Models at the cellular level

At the cellular level, the behaviors of cell–cell interaction, cell proliferation and migration are mainly modeled as follows.

2.1.1 Cell–cell interactions

When two cells interact including contact (Fig. 2A, B) and separation (Fig. 2C, D), for the sake of simplicity, we assume that the interaction of the two cells does not resist their relative rotation. Thus, a concentrated force only acts on each cell, and the forces on the two cells are equal but in opposite directions. Furthermore, the force is expressed by the Kelvin–Voigt model with a Hookean elastic spring and a Newtonian dashpot connected in parallel. Wherein, the elastic force produced by the Hookean elastic spring is decomposed into normal and shear components with normal and shear stiffnesses, and the normal stiffness is assumed to be three times of the shear stiffness (Canetta et al. 2005). Similarly, the damping force by the Newtonian dashpot is also decomposed into normal and shear components with the normal and shear critical damping ratios, see Fig. 2.

When two cells contact, we further assume that the forces on the cells are proportional to the contact (or overlapping) height at the contact location. The conversion relationship between the physical parameters of cells and the contact parameters is presented in Supporting Material [S3]. In the normal direction (Fig. 2A), the normal component F_{nij} of the contact force F_{ij} is given by:

$$F_{nij} = \left(-k_n \alpha - \eta_n v \cdot n\right) \cdot n \tag{1}$$

where k_n and η_n are the normal stiffness and critical damping ratio between the two cells (i, j). n denotes the normal unit vector along the line connecting the centers of the two cells. α notes the relative displacement in the normal direction. v

notes the relative velocity vector between the two cells. In the shear direction (Fig. 2B), we assume that a constant elastic force by the Hookean spring is kept and relative slippage between the two cells occurs, when the shear component is beyond the critical Coulomb's friction. The shear component F_{sij} of the contact force before- and after-slippage is given by:

$$\begin{aligned} F_{sij} &= -\mu \left|F_{nij}\right| \cdot t & \left|F_{sij}\right| &\geq \left|F_{nij}\right| \cdot \mu \\ F_{sij} &= \left(-k_s \beta - \eta_s v \cdot t\right) \cdot t & \left|F_{sij}\right| &< \left|F_{nij}\right| \cdot \mu \end{aligned} \tag{2}$$

where t is the tangent unit vector, μ, k_s and η_s are the friction coefficient, the shear stiffness and critical damping ratio between the two cells, respectively. β denotes the two cells' tangential relative displacement. v is the two cells' relative velocity vector. Then, the resultant force F_i of the cell i contact with N surrounding cells is expressed as:

$$F_i = \sum_{j}^{N} \left(F_{nij} + F_{sij}\right), \quad (j = 0, 1, 2, \ldots, N) \tag{3}$$

When two cells depart (Fig. 2C, D), the cell–cell interaction is modeled by an adhesion force yielded by CAFs in ECM, which drags the two cells to resist their separation. The adhesion behavior between the two cells is modeled as a bond, which consists of Hookean spring and Newtonian dashpot components, similar to the cell–cell contact model. However, the bond fails when the cell–cell separation force is over a critical adhesion force; in other words, the cell–cell interaction disappears. The expression of the adhesion force caused by CAFs is given by normal direction (Fig. 2C):

$$\begin{aligned} \overline{F}_{nij} &= \left(-\overline{k}_n \overline{\alpha} - \overline{\eta}_n v \cdot n\right) \cdot n & \left|\overline{F}_{nij}\right| &\leq \Omega_n \\ \overline{F}_{nij} &= 0 & \left|\overline{F}_{nij}\right| &> \Omega_n \end{aligned} \tag{4}$$
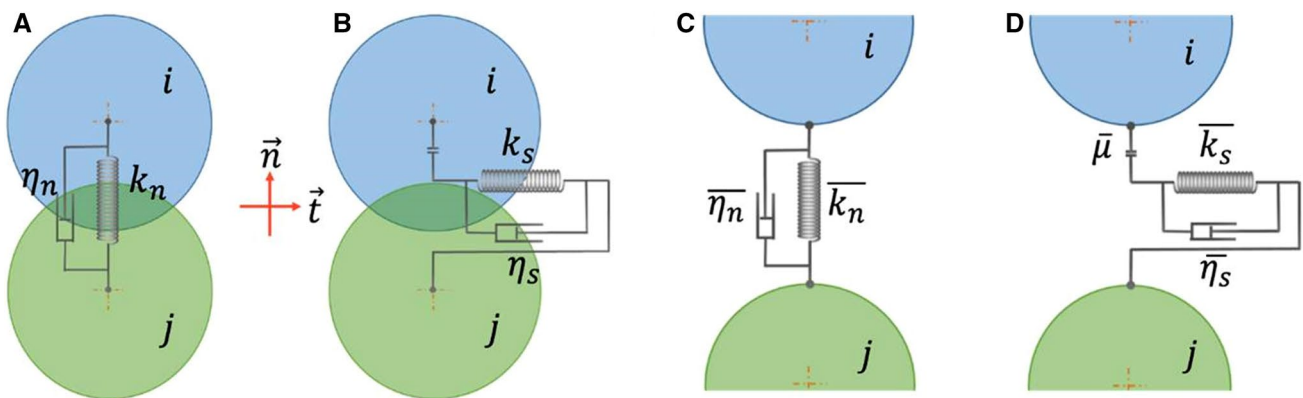

Fig. 2 Cell–cell interaction model. **A, B** The contact model of two cells, $\vec{n}$, denotes the normal unit vector along the line connecting the centers of the two cells (i, j). k_n and η_n are the normal stiffness and critical damping ratio between the two cells, respectively. $\vec{t}$ is the tan-gent unit vector, $\bar{\mu}$, k_s and η_s are the friction coefficient, the shear stiffness and critical damping ratio between the two cells, respectively. **C, D** The separation model of two cells, the symbols with a bar represent the corresponding parameters in **A, B**

Shear direction (Fig. 2D):

$$\begin{aligned} \overline{\boldsymbol{F}}_{sij} &= \left(-\bar{k}_s\bar{\beta} - \bar{\eta}_s\boldsymbol{v}\cdot\boldsymbol{t}\right)\cdot\boldsymbol{t} \quad \left|\overline{\boldsymbol{F}}_{sij}\right| \le \Omega_s \\ \overline{\boldsymbol{F}}_{sij} &= 0 \qquad\qquad\qquad\quad \left|\overline{\boldsymbol{F}}_{sij}\right| > \Omega_s \end{aligned} \tag{5}$$

where Ω_n and Ω_s are the critical normal and shear adhesion forces between the two cells. Then, the resultant force $\overline{\boldsymbol{F}}_i$ of the cell i with N surrounding cells,

$$\overline{\boldsymbol{F}}_i = \sum_j^N \left(\overline{\boldsymbol{F}}_{nij} + \overline{\boldsymbol{F}}_{sij}\right), \quad (j = 0, 1, 2, \ldots, N) \tag{6}$$

Combining Eqs. 3 and 6, the resultant force of a cell can be obtained according to the above contact and separation models. Finally, for the TC and HC, their resultant forces $\boldsymbol{F}_{\mathrm{TC}}$ and $\boldsymbol{F}_{\mathrm{HC}}$ are, respectively, calculated as,

$$\boldsymbol{F}_{\mathrm{TC}} = \sum \left(\boldsymbol{F}_{\mathrm{HC}\to\mathrm{TC}} + \boldsymbol{F}_{\mathrm{TC}\to\mathrm{TC}} + \boldsymbol{F}_{\mathrm{ECM}\to\mathrm{TC}} + \boldsymbol{F}_{\mathrm{Wall}\to\mathrm{TC}} + \overline{\boldsymbol{F}}_{\mathrm{HC}\to\mathrm{TC}} + \overline{\boldsymbol{F}}_{\mathrm{TC}\to\mathrm{TC}}\right) \tag{7}$$

$$\boldsymbol{F}_{\mathrm{HC}} = \sum \left(\boldsymbol{F}_{\mathrm{HC}\to\mathrm{HC}} + \boldsymbol{F}_{\mathrm{TC}\to\mathrm{HC}} + \boldsymbol{F}_{\mathrm{ECM}\to\mathrm{HC}} + \boldsymbol{F}_{\mathrm{Wall}\to\mathrm{HC}} + \overline{\boldsymbol{F}}_{\mathrm{HC}\to\mathrm{HC}} + \overline{\boldsymbol{F}}_{\mathrm{TC}\to\mathrm{HC}}\right) \tag{8}$$

where the arrows in the subscript of the force components represent the action of the former on the latter.

2.1.2 TC proliferation

Since this study focuses on the effect of the mechanical microenvironment on the early stage of tumor invasion, the physiological behaviors of TCs influenced by the mechanical microenvironment are considered only, and their weak responses to chemical factors (e.g., hypoxia and acidity) are neglected. An experiment has evidenced that the cell cycle of TCs was affected by local mechanical microenvironment, and the TCs did not proliferate and became solitary when the stress level was over 100 Pa (Roose et al. 2003). This experimental finding is employed to describe the physiological behavior of TCs during the early tumor invasion in our model. Specifically, the TCs are active and proliferable when the stress level is lower than 100 Pa; otherwise, the TCs are solitary. It is worth mentioning that the solitary TCs do not undergo apoptosis and they keep interacting with the surrounding cells. The proliferation of TCs is implemented by creating another TC at its original location to form two daughter TCs. Immediately after the creation, the two daughter TCs are completely overlapped; then, according to the cell–cell contact model (Fig. 2A, B), there is a great contact force, which leads to the migrations of the daughter TCs (Chaplain et al. 2006).

2.1.3 Cell migration

The Newton's second law of motion is used here to describe the cell migration. First, at a time t, employing the cell–cell interaction forces in Eqs. (7–8) and the cell mass calculated by the cell density and volume, we obtain the cell acceleration. Then, with a time incremental Δt, we solve the cell displacement through integrating the cell acceleration twice. After that, the cell migration path indicated by the displacement is determined. Furthermore, the new cell–cell interaction force is updated, and correspondingly, the updated forces at time $(t + \Delta t)$ are calculated by Eqs. (7–8). The iterative processes stop when the solid stresses balance among the HC, the TC and the discretized ECM, and the relative error of the interaction forces between two adjacent time steps is less than 10^{-3}.

2.2 Model at the tissue level

The applied external stresses are generated by expanding of the simulation region, which represents the tumor invasion against the surrounding tissue (outside the square boundary, Fig. 1). As the tumor invades, the external stresses increase. The surrounding tissue is assumed to be a linear-elastic material with a constant stiffness. Therefore, the external stress can be calculated based on the expanded boundary and the stiffness of the surrounding tissue. The external stress by the surrounding tissue and the solid stress by the invading tumor inside the simulation region reach a balance at the expanding boundary. The criterion of the balance is when all the cells and the discretized ECM contacting with the boundary meet a judgment, i.e., the relative error of the interaction forces between two adjacent time steps is less than 10^{-3}.

2.3 Integration of the cellular level and the tissue level

Since the cell displacement and cell–cell interaction are discrete at the cellular level and cannot be transferred directly to a continuum model at the tissue level, we divided the simulation region into 225 lattices. For each lattice, all the interactions between HCs, TCs and discretized ECM were averaged. With the averaging procedure, the integration between the cellular level and the tissue level is achieved.

The average stress $\bar{\sigma}$ in a lattice of space S is computed as (Christoffersen et al. 1981):

$$\bar{\sigma} = -\frac{1}{S} \sum_{N_c} \boldsymbol{F}^{(c)} \otimes \boldsymbol{L}^{(c)} \tag{9}$$

where N_c is the number of interactions between HCs, TC, S and discretized ECM that lie in the measured lattice. $\boldsymbol{F}^{(c)}$ is the interaction force vector. $\boldsymbol{L}^{(c)}$ is the branch vector joining the centers of two interactive cells. $\otimes$ denotes outer product. The compressive stress is defined to be negative. The underlying assumption for Eq. (9) indicates a static analysis. Thus, the solid stress field of the simulation region is calculated when the forces between the HCs, the TCs and the discretized ECM are all in balance.

2.4 Numerical simulation

Here, we treated 15 stages during the early tumor invasion. In each stage, only one TC-division cycle is assumed, and all active TCs are assumed to simultaneously start proliferating. At the beginning of the simulation, the HCs and ECM within the simulation region are randomly generated with densities of 0.334 Unites/(10 μm)^2 and 4.671 Unites/(10 μm)^2, respectively. Moreover, one of the HCs is assumed to mutate to TC, and the mechanical properties of the HC are changed to those of the TC. Furthermore, the TC starts proliferating and induces solid stress inside the simulation region. The force and displacement are calculated by an iteration, and with the calculated force and displacement, the morphology of the invasive tumor is updated. After the solid stress is balanced by the applied external stress at the expanding boundary, the two stresses reach equilibrium, and the next stage starts. We assume that all the cells and elements are restricted within the square simulation region and only have mechanical interactions with the surrounding tissue. The simulation ends after completing the 15 stages, and the TCs are almost fully stacked in the region. The iterative flowchart of the simulation is illustrated in Fig. 3.

3 Results

3.1 The dynamics of tumor invasion and the solid stress field

Figure 4 displays the dynamics of the tumor invasion into the host tissues and the corresponding growth-induced first principal solid stress field at eight time points ($T = 1, 3, 5, 7, 9, 11, 13, 15$). The red elements in the square simulation region represent the active TCs, while the dark red, blue and pink ones represent solitary TCs, HCs and ECM, respectively. Since the boundary (black lines represent the boundaries) of
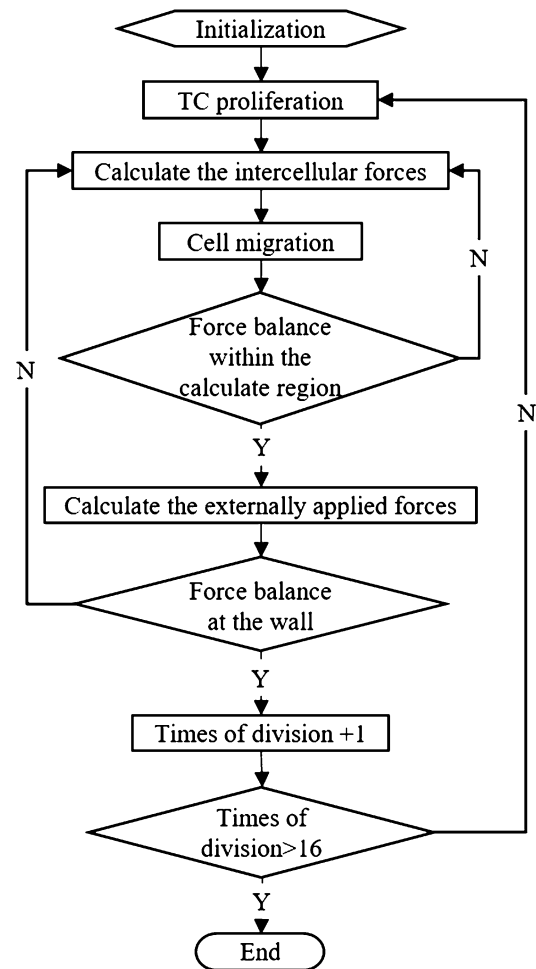

Fig. 3 Flowchart of the iterative algorithm

the region is expandable, the region is obviously extended due to tumor invasion. The solitary TCs firstly emerge in the central area at $T = 6$, and the number of the solitary TCs gradually increases as the tumor grows. At the end of the simulation ($T = 15$), most of the TCs become solitary due to the elevated first principal solid stresses, which exceed the critical stress 100 Pa. Moreover, the fields of the first principal solid stress at the eight time points are also mapped. From the mapped field, we can see that the first principal solid stress is not uniformly distributed during tumor invasion. In particular, the high-stress areas are scattered in the tumor center. This result is more realistic and is different from the results of the previous models which often show a uniform interstitial hypertension at tumor center and a low stress or pressure at the periphery.

The changes in the numbers of active and solitary TCs during tumor invasion are shown in Fig. 5A. The number of the active TCs approaches a constant, whereas the number of the solitary TCs increases sharply due to the increase in the principal solid stress level to over 100 Pa after $T = 9$
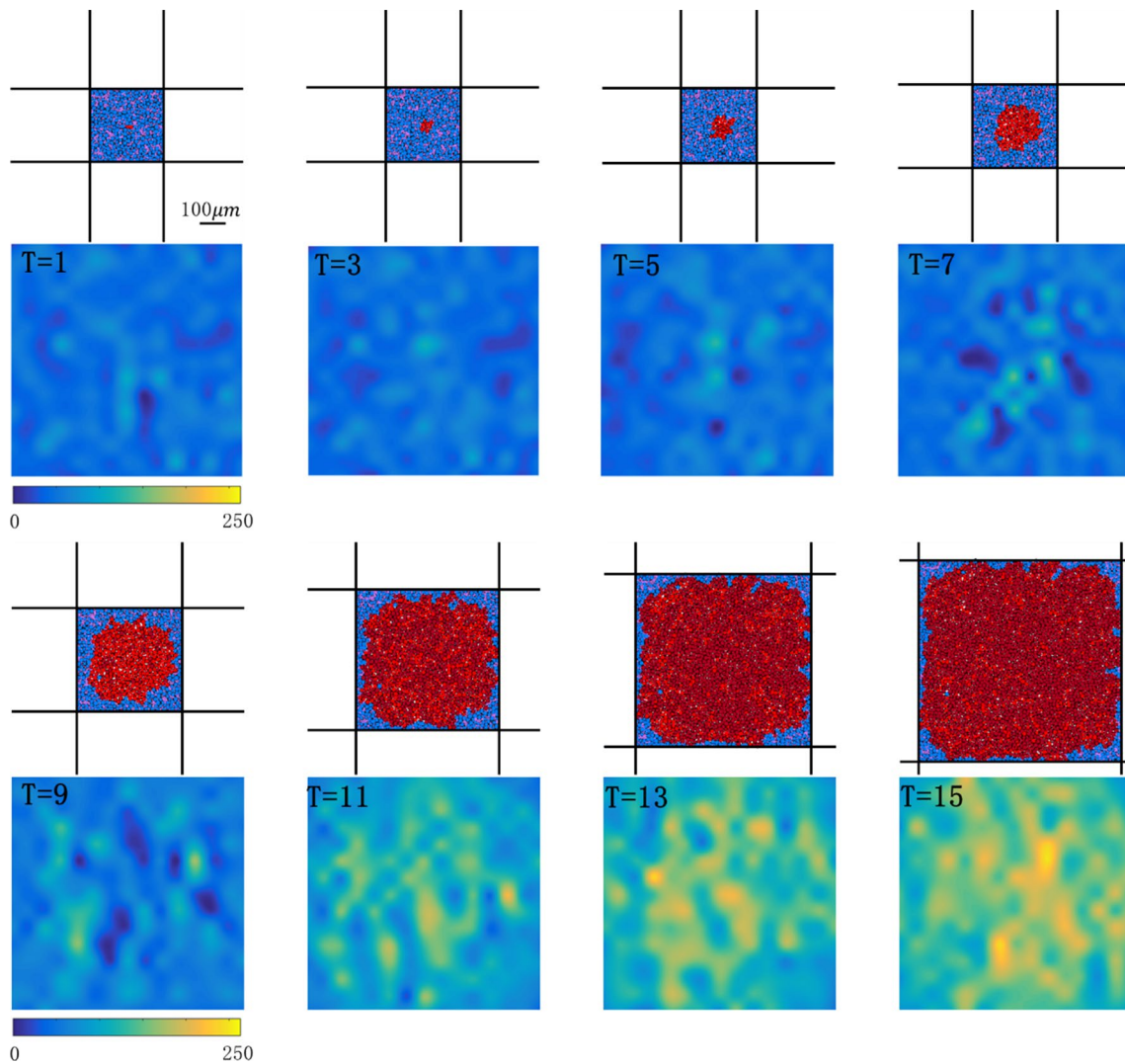
Fig. 4 Dynamic evolutions of tumor morphology and the corresponding first principal solid stress field during the simulation of tumor invasion
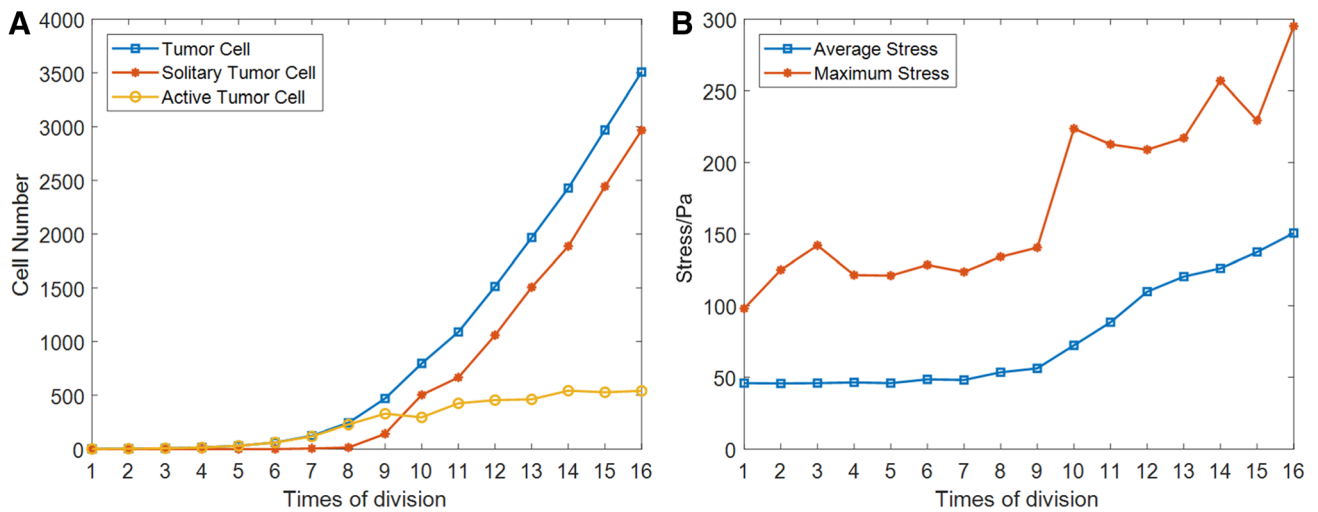

Fig. 5 Variations of **A** TC number, **B** average and maximum stresses in the simulation region during tumor invasion

(Fig. 5B). At the end of the simulation, the total number of TCs is over 3500, in which the solitary TCs account for over 80%. Figure 5B shows the average and the maximum principal solid stresses in the simulation region. The results are in consistent with an experimental observation which showed a similar increase pattern in the solid stress in the breast cancer (Triantafyllos et al. 2013). Note that the maximum principal solid stress fluctuates rather than monotonically increases during tumor invasion. This further demonstrates the heterogeneity of the solid stress distribution caused by TC proliferation and tumor invasion, which is believed to be one of the important features of the abnormal mechanical microenvironment in tumors.

The cell–cell interaction is elaborately shown in Fig. 6A. The blue lines inside the tumor represent the compressive contacts; in other words, the TCs in the tumor are mainly in compression. The yellow ones around the tumor periphery represent the tensile contacts. A similar pattern was also demonstrated by previous experimental findings (Triantafyllos et al. 2013; Nia et al. 2017); particularly, Nia et al. (2017) presented the growth-induced tensile stress distribution at the tumor periphery based on their analysis of a mouse breast tumor and a mathematical model (Fig. 6B).

3.2 Decreases in TC/ECM stiffness promote tumor growth

To investigate the effect of TC stiffness on the tumorigenesis within a host tissue, we performed additional simulations by varying the normal stiffness of the TCs and maintaining the shear stiffness as one-third of the normal one. Compared to the TC stiffness of 500 Pa in the baseline model, the decrease in TC stiffness leads to an exponential increase in TC number (Fig. 7A), and consequently, the TCs occupy a large domain within the tissue (Fig. 7B). The total TC number in the case of the TC stiffness at 300 Pa is about twice of that in the baseline case. This finding is consistent

with other simulations and experimental observation (Baker et al. 2010). Furthermore, both the growth-induced average solid stress (Fig. 7C) and the applied external stress from the surrounding tissue (Fig. 7D) increase due to the rapid tumor invasion when the TC stiffness decreases.

ECM stiffness is believed to activate the intracellular signaling pathways to regulate the cell behavior, and further influences tumorigenesis and metastasis (Schedin and Keely 2011). To study the impact of ECM stiffness, we performed a parametric analysis by changing the ECM stiffness from 300 to 1200 Pa. Similar to the effect of the TC stiffness, a decrease in ECM stiffness results in an increase in TC proliferation (Fig. 8A). However, the ECM stiffness weakly influences the tumor growth (Fig. 8B), as well as the average solid stress (Fig. 8C) and applied external stress (Fig. 8D).

3.3 Stiffening of the surrounding tissue inhibits tumor growth and invasion

In vitro experimental models have been developed to mimic the solid stress in the tumor microenvironment (Kalli and Stylianopoulos 2018). These models consisted of tumor spheroids growth in a confined environment (polymer ECM or elastic capsules) that caused the increase in the applied external stress (Cheng et al. 2011). In our model, the applied external stress is determined by the stiffness of the surrounding tissue and balanced by the growth-induced solid stress at the boundary between the simulation region and the surrounding tissue. When the stiffness of the surrounding tissue (167 Pa in the baseline model, Graziano and Preziosi 2007) increases, the TC proliferation and tumor invasion are apparently inhibited, as shown in Fig. 9A, B. Although the reduced average solid stress with a stiffer surrounding tissue is seen at the late stage of the simulation (Fig. 9C), the simulation region is still subjected to a high applied stress from the surrounding tissue during tumor invasion, which may be attributed to an increased TC apoptosis. This is also

Fig. 6 Cell–cell contact states at the cellular level in the simulation (**A**) and 2D stress states in a cross section of a mouse breast tumor in Nia et al.'s study (Nia et al. 2017) (**B**)
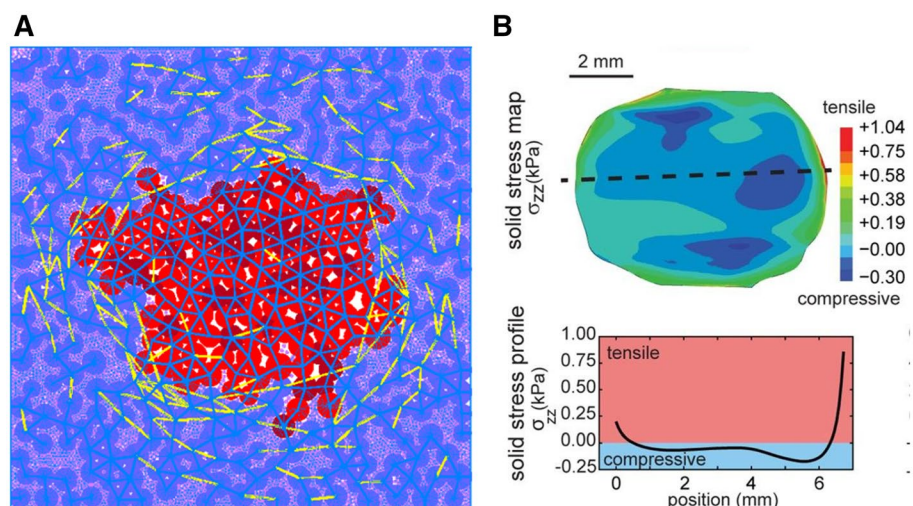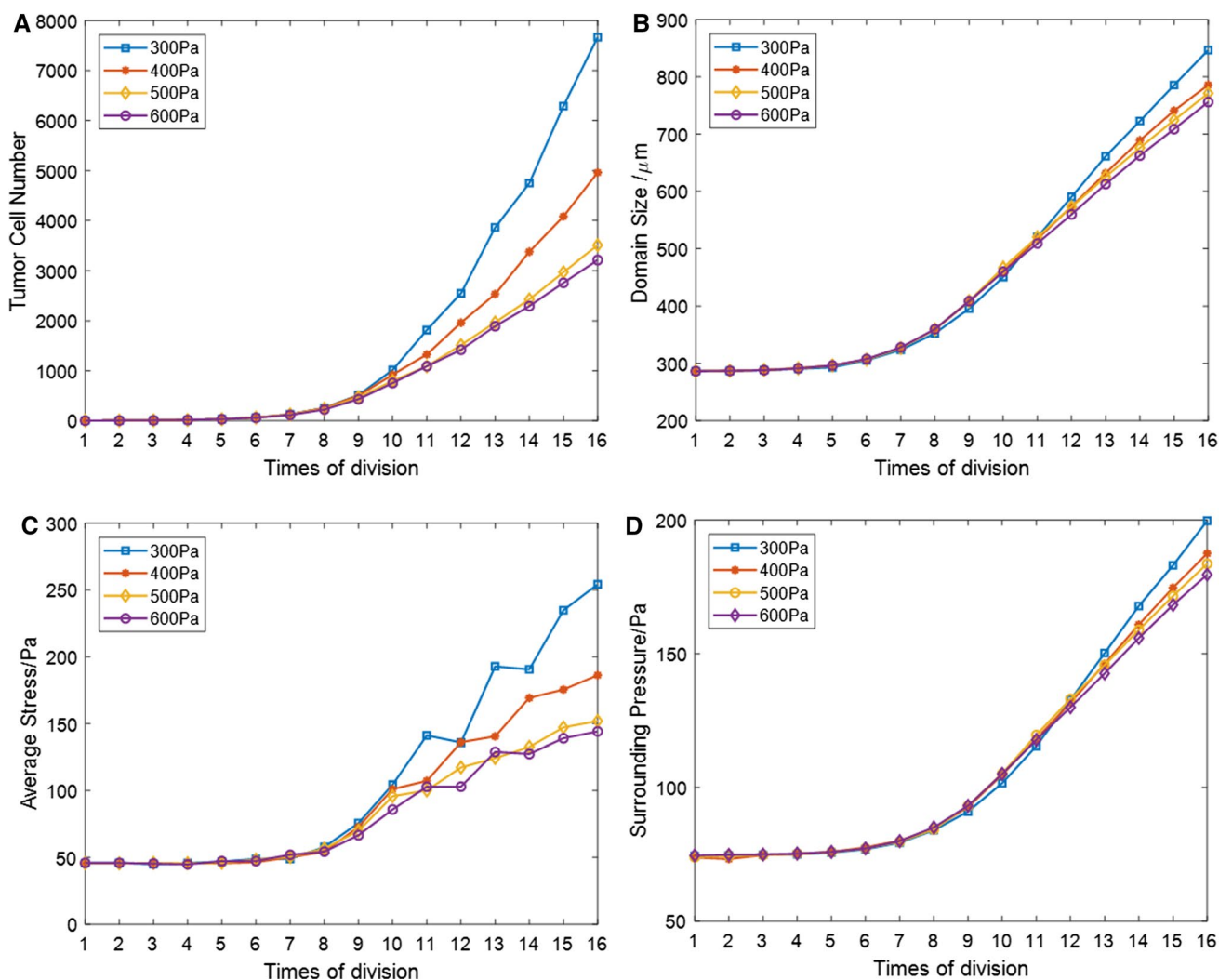
Fig. 7 Influence of the TC stiffness on tumor growth and stress

in consistent with the in vitro experimental observations (Tse et al. 2012). When the stiffness of the surrounding tissues increases, the tumor tissue will be subjected to higher pressure to expand outward with the same size, leading to greater stress in the simulation area. Meanwhile, as the hypothesis presented in this paper, when the resultant force subject on an individual tumor cell is greater than the assumed threshold (100 Pa, Roose et al. 2003), its physiological state changes from active state to solitary state. Therefore, most tumor cells transfer to solitary phenotype and stop proliferation, resulting in the significant decrease in tumor cell number and tumor expansion in the case of stiffer surrounding tissue (250 Pa), as shown in Fig. 9A, B. As the number of tumor cells decreases, the expansion size of the simulation region decreases due to tumor proliferation, which in turn reduces the deformation of surrounding tissues and reduces the average pressure increment of the computational region. Consequently, the increase

in average stress and surrounding pressure are not obvious in the case of 250 Pa, as shown in Fig. 9C, D.

3.4 Mechanical factors regulate tumor invasiveness

Here, tumor invasiveness is represented by the irregularity of the tumor morphology. To quantitatively analyze tumor invasiveness, we first delineated a circle whose area is equal to the tumor area (red parts in Fig. 10). A parameter M is introduced as a ratio between the invasion area and the tumor area, and the invasion area is defined as the sum of the TCs area outside the circle and non-TCs (or blank) area inside the circle. Therefore, a greater M indicates that tumors are more easily to invade into the healthy tissue, or a higher invasiveness. The effects of the stiffnesses of the TC, the ECM, the surrounding tissues and the CAF strength on the invasiveness are investigated. Figure 10 shows that a stiffer TC or ECM leads to a more invasive tumor, even though it slows down the tumor
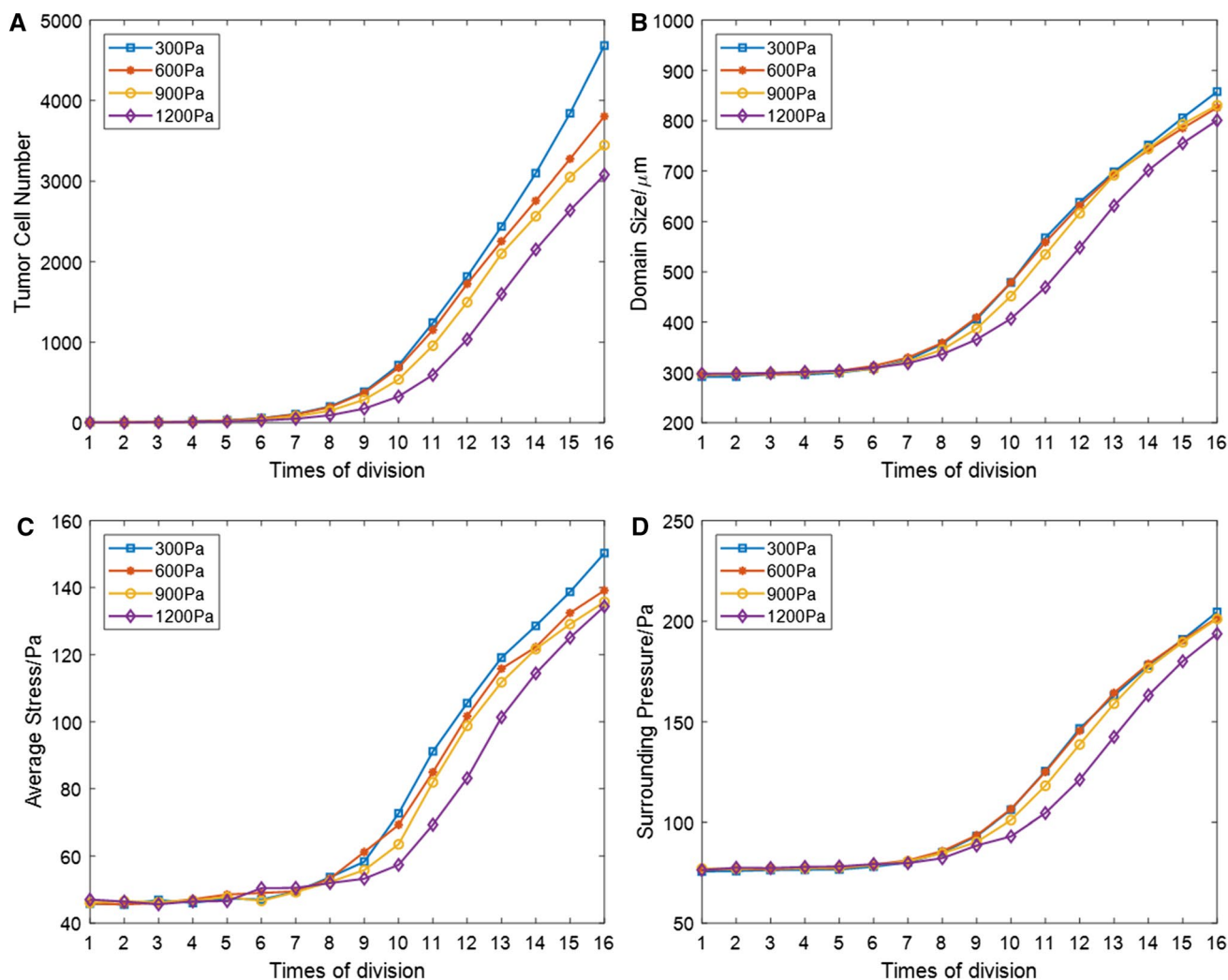
Fig. 8 Influence of the ECM stiffness on tumor growth and stress

growth as we presented in Sect. 3.2. This suggests the Janus face of the mechanical microenvironment on tumor invasion and growth. On the one hand, a compliant TC or ECM is beneficial for tumor growth and TC proliferation; on the other hand, a stiff TC or ECM may be associated with a high tumor invasiveness. In addition, we also changed the CAF strength to assess the influence of cell–cell adhesion on tumor invasiveness. It was found that a smaller in CAF strength, indicating a weaker adhesion between cells, resulted in a more aggressive tumor invasion, and a finger-like invasive morphology could be easily seen (Fig. 10).

4 Discussions

Numerous experiments have shown multiple cancerous phenomena are induced by both biophysical and biochemical stimulations. Previous studies have revealed the

underlying biochemical factors and signal pathways that relate to TC proliferation and migration. However, the observed cross-scale phenomena remain disconnected, and the underlying mechanism is still elusive. The mechanical microenvironment is well accepted as a crucial factor in tumor growth and metastasis, and previous literature explicitly reported that cells would not move if the complex physical–biochemical microenvironment did not produce proper mechanical forces. Since it is challenging to measure the heterogeneous solid stress field in tumor tissues, we established a multiscale biomechanical model to investigate the dynamic changes of the growth-induced solid stress field during the early tumor growth. Moreover, we investigated the specific mechanical factors that regulate the early tumor growth and invasion.

Most existing cell-based discrete models are only able to treat a limited cell number to study the mechanical microenvironment of a tumor, or use a discrete–continuous hybrid
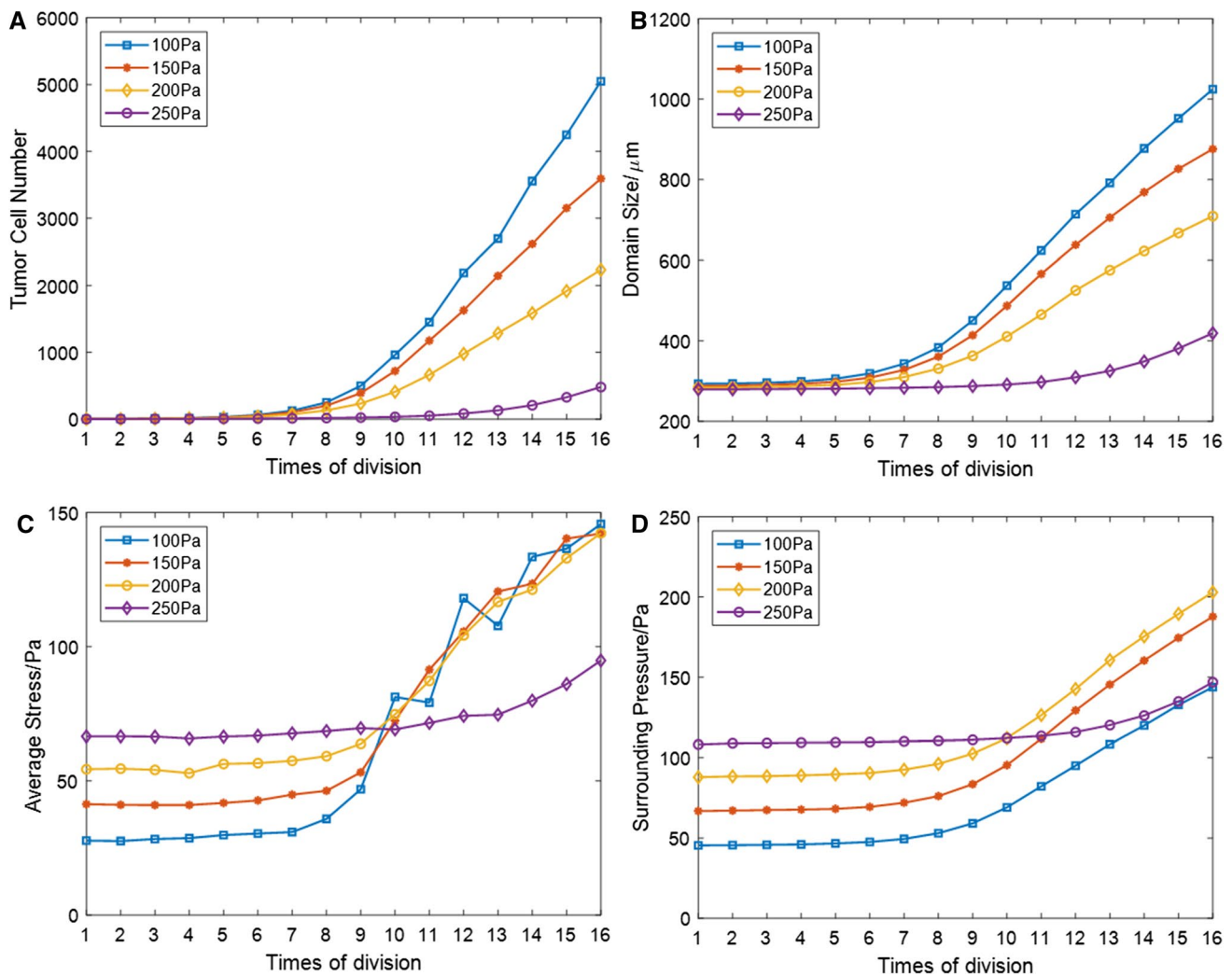
Fig. 9 Influence of the stiffening in the surrounding tissue on tumor growth and stress

model to reduce the computational cost. Different from these models, we proposed a novel method to describe the growth-induced solid stress field by considering the contact interactions of a single cell with its neighboring elements. Furthermore, an off-lattice multiscale model is developed to integrate tumor mechanical microenvironment and TC proliferation. At the cellular level, the force–displacement relationship describing the intercellular contact satisfies the Kelvin–Voigt viscoelastic model, which consists of a Hookean elastic spring and a Newtonian dashpot to describe the elastic and the viscous behaviors, respectively. Then, we use the Newton's second law of motion to update the location of each cell. At the tissue level, we consider that the growth-induced solid stresses are balanced by the applied external stresses from the surrounding tissue. Expanding boundary is applied to reflect the tumor growth as a result of the TC proliferation.

This multiscale model quantitatively describes how and to what extent the microscopic mechanical microenvironment induces the changes of the macroscopic tumor morphology and allows stress analysis at the tissue level. Starting from a single TC, we investigated the dynamic tumor invasion into a healthy tissue, as well as the distribution of the growth-induced solid stress during tumorigenesis. The dynamic stress field calculated from the model reveals a heterogeneous solid stress distribution within the proliferating tumor. In addition, compressive stresses were found at the center region and tensile stresses around the tumor periphery, which is consistent with the in vitro experimental results (Emon et al. 2018). The present model provides a theoretical tool to investigate the dynamic changes in the mechanical environment during tumor growth and invasion.

Moreover, the model allows investigation on the roles of specific mechanical factors on the invasive morphology of
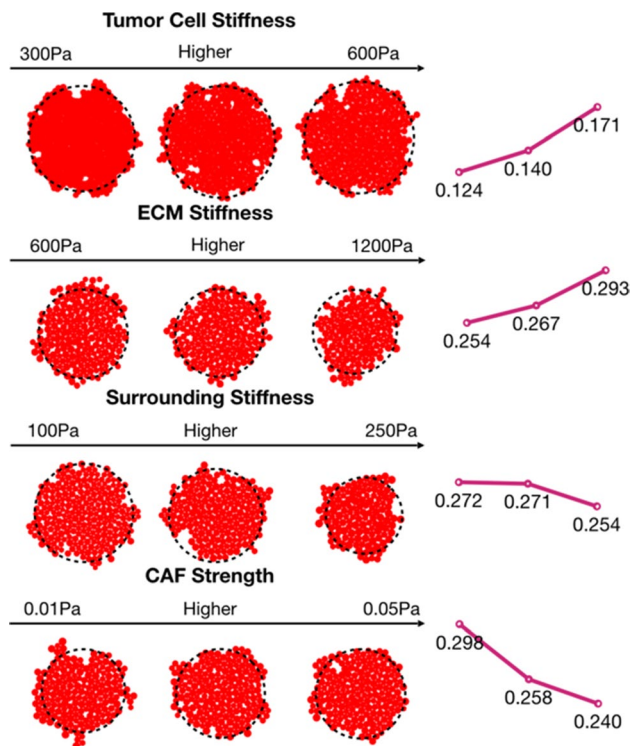
Fig. 10 Impact of mechanical factors on tumor invasiveness. Note: The left column represents the tumor morphologies ($T=8$) under three different mechanical factors, and polylines on the right are their M values, which represent the deferent degrees of invasiveness under the three different mechanical factors

tumor. For example, we studied how the stiffness of either the TCs or the matrix affected the tumor growth. With a reduction in stiffness of either TC or the matrix, the resisting force against invasion decreases. In contrast, compliant TCs promote tumor growth. However, the simulation results also suggest that stiffer TCs and ECM as well as compliant surrounding tissues contribute to a more invasive pattern of tumor morphology. This finding is interesting and can be used to explain the phenomena explored in in vitro experimental studies (Gkretsi et al. 2017). In the experiment, stiffening ECM has been shown to upregulate cell-ECM adhesion protein (e.g., Ras suppressor-1), which limits tumor invasion and induces CAF activation and TC migration, thus leading to a fibrotic response. Despite the consistency with the experimental observations, more experimental data are still needed to fully understand the dynamic interactions between ECM stiffening and intercellular adhesion.

Furthermore, the model helps us to understand how the mechanical microenvironment affects tumor invasion, which was represented by a morphological parameter M. It is noteworthy that a reduction in CAF strength can dramatically enhance the invasiveness, from 0.240 to 0.298 in M, and eventually form a finger-like invasion morphology. In fact,

it has been demonstrated that CAFs can mediate the invasiveness of colon, pancreatic and breast cancer cells when co-injected into mice (Hwang et al. 2008; Karagiannis et al. 2012; Xu et al. 2016). This indicates the potential therapy by inhibiting the CAFs and disrupting the CAF-associated paracrine growth factor signals (LeBleu and Kalluri 2018; Ziani et al. 2018). In this context, the present study revealed the quantitative effects of the CAFs strength on tumor invasion, which may act as pharmaceutical target in order to prohibit tumor growth and metastasis.

Finally, this model is multipotential because of its extendibility. For instance, the TC responses depend not only on the intercellular forces but also on the biochemical factors. Thus, it could be extended to include the biochemical microenvironment to generate the chemotactic gradients for cell movement, and the tumor growth dynamics under the chemical microenvironment can be described by employing reaction–diffusion equations (Xue et al. 2016, 2017; Yin et al. 2019). Also, by considering the actions at the molecular level such as gene expression and signaling pathways, we can extend the model to identify what subcellular events contribute to the macroscopic mechanical microenvironment of the tumor.

5 Conclusions

In this study, we proposed a multiscale mathematical model to bridge the gap between the cell–cell interactions at the cellular level and the mechanical microenvironment at the tissue level during the early stage of tumor growth. The model describes the dynamic changes of the growth-induced solid stress field and tumor invasion in response to dynamic mechanical microenvironment. The simulation results show that an increase in the compliance of TCs and matrix can cause TCs to proliferate at a much faster rate and invade to surrounding tissue more easily. Meanwhile, the stiffening of TCs and matrix contributes to aggressive morphology of tumor invasion. The proposed model can be served as a theoretical platform to study the underlying mechanism of the mechanical microenvironmental factors during early tumor invasion and metastasis.

Compliance with ethical standards

Conflict of interest The authors declare that they have no conflict of interest.

References

Ambrosi D, Mollica F (2002) On the mechanics of a growing tumor. Int J Eng Sci 40:1297–1316. https://doi.org/10.1016/S0020-7225(02)00014-9

Ambrosi D, Preziosi L (2009) Cell adhesion mechanisms and stress relaxation in the mechanics of tumours. Biomech Model Mechanobiol 8:397–413. https://doi.org/10.1007/s10237-008-0145-y

Anderson ARA (2005) A hybrid mathematical model of solid tumour invasion: the importance of cell adhesion. Math Med Biol J IMA 22:163–186. https://doi.org/10.1093/imammb/dqi005

Baish JW, Stylianopoulos T, Lanning RM, Kamoun WS, Fukumura D, Munn LL, Jain RK (2011) Scaling rules for diffusive drug delivery in tumor and normal tissues. Proc Natl Acad Sci USA 108:1799–1803. https://doi.org/10.1073/pnas.1018154108

Baker EL, Lu J, Yu DH, Bonnecaze RT, Zaman MH (2010) Cancer cell stiffness: integrated roles of three-dimensional matrix stiffness and transforming potential. Biophys J 99:2048–2057. https://doi.org/10.1016/j.bpj.2010.07.051

Branton MH, Kopp JB (1999) TGF-β and fibrosis. Microbes Infect 1:1349–1365. https://doi.org/10.1016/S1286-4579(99)00250-6

Butcher DT, Alliston T, Weaver VM (2009) A tense situation: forcing tumour progression. Nat Rev Cancer 9:108–122. https://doi.org/10.1038/nrc2544

Canetta E, Duperray A, Leyrat A, Verdier CJB (2005) Measuring cell viscoelastic properties using a force-spectrometer: influence of protein–cytoplasm interactions. Biorheology 42:321–333. https://doi.org/10.1016/j.bbmt.2004.10.003

Chaplain MAJ, Graziano L, Preziosi L (2006) Mathematical modelling of the loss of tissue compression responsiveness and its role in solid tumour development. Math Med Biol J IMA 23:197–229. https://doi.org/10.1093/imammb/dql009

Chen Y, Wise SM, Shenoy VB, Lowengrub JS (2014) A stable scheme for a nonlinear, multiphase tumor growth model with an elastic membrane. Int J Numer Methods Biomed Eng 30:726–754. https://doi.org/10.1002/cnm.2624

Cheng G, Tse J, Jain RK, Munn LL (2011) Micro-environmental mechanical stress controls tumor spheroid size and morphology by suppressing proliferation and inducing apoptosis in cancer cells. PLoS ONE 4:e4632. https://doi.org/10.1371/journal.pone.0004632

Christoffersen J, Mehrabadi MM, Nematnasser S (1981) A micromechanical description of granular material behavior. J Appl Mech Trans ASME 48:339–344. https://doi.org/10.1115/1.3157619

Demou ZN (2010) Gene expression profiles in 3D tumor analogs indicate compressive strain differentially enhances metastatic potential. Ann Biomed Eng 38:3509–3520. https://doi.org/10.1007/s10439-010-0097-0

Drasdo D, Hohme S (2005) A single-cell-based model of tumor growth in vitro: monolayers and spheroids. Phys Biol 2:133–147. https://doi.org/10.1088/1478-3975/2/3/001

Emon B, Bauer J, Jain Y, Jung B, Saif T (2018) Biophysics of tumor microenvironment and cancer metastasis—a mini review. Comput Struct Biotechnol J 16:279–287. https://doi.org/10.1016/j.csbj.2018.07.003

Fraldi M, Carotenuto AR (2018) Cells competition in tumor growth poroelasticity. J Mech Phys Solids 112:345–367. https://doi.org/10.1016/j.jmps.2017.12.015

Gkretsi V, Stylianou A, Louca M, Stylianopoulos T (2017) Identification of Ras suppressor-1 (RSU-1) as a potential breast cancer metastasis biomarker using a three-dimensional in vitro approach. Oncotarget 8:27364–27379. https://doi.org/10.18632/oncotarget.16062

Graziano L, Preziosi L (2007) Mechanics in tumor growth. In: Mollica F, Preziosi L, Rajagopal KR (eds) Modeling of biological materials. Springer, Boston, pp 263–321. https://doi.org/10.1007/978-0-8176-4411-6_7

Hatzikirou H, Brusch L, Schaller C, Simon M, Deutsch A (2010) Prediction of traveling front behavior in a lattice-gas cellular automaton model for tumor invasion. Comput Math Appl 59:2326–2339. https://doi.org/10.1016/j.camwa.2009.08.041

Helmlinger G, Netti PA, Lichtenbeld HC, Melder RJ, Jain RK (1997) Solid stress inhibits the growth of multicellular tumor spheroids. Nat Biotechnol 15:778–783. https://doi.org/10.1038/nbt0897-778

Huang Y, Goel S, Duda DG, Fukumura D, Jain RK (2013) Vascular normalization as an emerging strategy to enhance cancer immunotherapy. Can Res 73:2943–2948. https://doi.org/10.1158/0008-5472.CAN-12-4354

Hwang RF et al (2008) Cancer-associated stromal fibroblasts promote pancreatic tumor progression. Can Res 68:918–926. https://doi.org/10.1158/0008-5472.can-07-5714

Ishihara S, Inman DR, Li WJ, Ponik SM, Keely PJ (2017) Mechanosignal transduction in mesenchymal stem cells induces prosaposin secretion to drive the proliferation of breast cancer cells. Can Res 77:6179–6189. https://doi.org/10.1158/0008-5472.Can-17-0569

Islam MT, Chaudhry A, Unnikrishnan G, Reddy JN, Righetti R (2018) An analytical poroelastic model for ultrasound elastography imaging of tumors. Phys Med Biol 63:025031. https://doi.org/10.1088/1361-6560/aa9631

Jain RK (2013) Normalizing tumor microenvironment to treat cancer: bench to bedside to biomarkers. J Clin Oncol 31:U2205–U2210. https://doi.org/10.1200/Jco.2012.46.3653

Jain RK, Martin JD, Stylianopoulos T (2014) The role of mechanical forces in tumor growth and therapy. Annu Rev Biomed Eng 16(16):321–346. https://doi.org/10.1146/annurev-bioeng-071813-105259

Jeon J, Quaranta V, Cummings PT (2010) An off-lattice hybrid discrete-continuum model of tumor growth and invasion. Biophys J 98:37–47. https://doi.org/10.1016/j.bpj.2009.10.002

Jeroen H et al (2006) Onset of abnormal blood and lymphatic vessel function and interstitial hypertension in early stages of carcinogenesis. Can Res 66:3360. https://doi.org/10.1158/0008-5472.CAN-05-2655

Kalli M, Stylianopoulos T (2018) Defining the role of solid stress and matrix stiffness in cancer cell proliferation and metastasis. Front Oncol 8:55. https://doi.org/10.3389/fonc.2018.00055

Kamoun WS et al (2010) Simultaneous measurement of RBC velocity, flux, hematocrit and shear rate in vascular networks. Nat Methods 7:655. https://doi.org/10.1038/nmeth.1475

Karagiannis GS, Poutahidis T, Erdman SE, Kirsch R, Riddell RH, Diamandis EP (2012) Cancer-associated fibroblasts drive the progression of metastasis through both paracrine and mechanical pressure on cancer tissue. Mol Cancer Res 10:1403–1418. https://doi.org/10.1158/1541-7786.Mcr-12-0307

Kaufman LJ, Brangwynne CP, Kasza KE, Filippidi E, Gordon VD, Deisboeck TS, Weitz DA (2005) Glioma expansion in collagen I matrices: analyzing collagen concentration-dependent growth and motility patterns. Biophys J 89:635–650. https://doi.org/10.1529/biophysj.105.061994

Kyriacou SK, Davatzikos C, Zinreich SJ, Bryan RN (1999) Nonlinear elastic registration of brain images with tumor pathology using a biomechanical model [MRI]. IEEE Trans Med Imaging 18:580–592. https://doi.org/10.1109/42.790458

LeBleu VS, Kalluri R (2018) A peek into cancer-associated fibroblasts: origins, functions and translational impact. Dis Models Mech 11:dmm029447. https://doi.org/10.1242/dmm.029447

MacLaurin J, Chapman J, Jones GW, Roose T (2012) The buckling of capillaries in solid tumours. Proc R Soc A Math Phys Eng Sci 468:4123–4145. https://doi.org/10.1098/rspa.2012.0418

Mallet DG, De Pillis LG (2006) A cellular automata model of tumor–immune system interactions. J Theor Biol 239:334–350. https://doi.org/10.1016/j.jtbi.2005.08.002

Montel F, Delarue M, Elgeti J, Vignjevic D, Cappello G, Prost J (2012) Isotropic stress reduces cell proliferation in tumor spheroids. New J Phys 14:055008. https://doi.org/10.1088/1367-2630/14/5/055008

Mueller-Klieser W (1987) Multicellular spheroids. A review on cellular aggregates in cancer research. Cancer Res Clin Oncol 113:101–122. https://doi.org/10.1007/BF00391431

Netti P, Baxter L, Coucher Y, Skalak R, Jain RJB (1995) A poroelastic model for interstitial pressure in tumors. Biorheology 32:346. https://doi.org/10.1016/0006-355X(95)92330-D

Nia HT et al (2017) Solid stress and elastic energy as measures of tumour mechanopathology. Nat Biomed Eng 1:0004. https://doi.org/10.1038/s41551-016-0004

Pankova D et al (2016) Cancer-associated fibroblasts induce a collagen cross-link switch in tumor stroma. Mol Cancer Res 14:287–295. https://doi.org/10.1158/1541-7786.Mcr-15-0307

Paszek MJ, Weaver VM (2004) The tension mounts: mechanics meets morphogenesis and malignancy. J Mammary Gland Biol Neoplasia 9:325–342. https://doi.org/10.1007/s10911-004-1404-x

Patel AA, Gawlinski ET, Lemieux SK, Gatenby RA (2001) A cellular automaton model of early tumor growth and invasion: the effects of native tissue vascularity and increased anaerobic tumor metabolism. J Theor Biol 213:315–331. https://doi.org/10.1006/jtbi.2001.2385

Pierre-Jean W, Boris H, Therapies M (2009) Myofibroblasts work best under stress. J Bodyw Mov Ther 13:121–127. https://doi.org/10.1016/j.jbmt.2008.04.031

Pries AR, Hopfner M, le Noble F, Dewhirst MW, Secomb TW (2010) The shunt problem: control of functional shunting in normal and tumour vasculature. Nat Rev Cancer 10:587–593. https://doi.org/10.1038/nrc2895

Ribeiro FL, Dos Santos RV, Mata AS (2017) Fractal dimension and universality in avascular tumor growth. J Phys Rev E 95:042406. https://doi.org/10.1103/PhysRevE.95.042406

Roose T, Netti PA, Munn LL, Boucher Y, Jain RK (2003) Solid stress generated by spheroid growth estimated using a linear poroelasticity model. Microvasc Res 66:204–212. https://doi.org/10.1016/s0026-2862(03)00057-8

Schedin P, Keely PJ (2011) Mammary gland ECM remodeling, stiffness, and mechanosignaling in normal development and tumor progression. Cold Spring Harb Perspect Biol 3:a003228. https://doi.org/10.1101/cshperspect.a003228

Smirnov P et al (2010) In vivo cellular imaging of lymphocyte trafficking by MRI: a tumor model approach to cell-based anticancer therapy. Magn Reson Med 56:498–508. https://doi.org/10.1002/mrm.20996

Stolarska MA, Kim Y, Othmer HG (2009) Multi-scale models of cell and tissue dynamics. Philos Trans R Soc A Math Phys Eng Sci 367:3525–3553. https://doi.org/10.1098/rsta.2009.0095

Triantafyllos S et al (2012) Causes, consequences, and remedies for growth-induced solid stress in murine and human tumors. Proc Natl Acad Sci USA 109:15101–15108. https://doi.org/10.1073/pnas.1213353109

Triantafyllos S, Martin JD, Matija S, Fotios M, Jain SR, Jain RK (2013) Coevolution of solid stress and interstitial fluid pressure in tumors during progression: implications for vascular collapse. Can Res 73:3833–3841. https://doi.org/10.1158/0008-5472.can-12-4521

Tse JM, Cheng G, Tyrrell JA, Wilcox-Adelman SA, Boucher Y, Jain RK, Munn LL (2012) Mechanical compression drives cancer cells toward invasive phenotype. Proc Natl Acad Sci USA 109:911–916. https://doi.org/10.1073/pnas.1118910109

Voutouri C, Mpekris F, Papageorgis P, Odysseos AD, Stylianopoulos T (2014) Role of constitutive behavior and tumor–host mechanical interactions in the state of stress and growth of solid tumors. PLoS ONE 9:e104717. https://doi.org/10.1371/journal.pone.0104717

Xu K, Tian XJ, Oh SY, Movassaghi M, Naber SP, Kuperwasser C, Buchsbaum RJ (2016) The fibroblast Tiam1-osteopontin pathway modulates breast cancer invasion and metastasis. Breast Cancer Res 18:14. https://doi.org/10.1186/s13058-016-0674-8

Xue SL, Li B, Feng XQ, Gao H (2016) Biochemomechanical poroelastic theory of avascular tumor growth. J Mech Phys Solids 94:409–432. https://doi.org/10.1016/j.jmps.2016.05.011

Xue SL, Li B, Feng XQ, Gao H (2017) A non-equilibrium thermodynamic model for tumor extracellular matrix with enzymatic degradation. J Mech Phys Solids 104:32–56. https://doi.org/10.1016/j.jmps.2017.04.002

Yazdi MR, Naghavi N, Hosseini F (2016) Numerical simulation of solid tumor invasion and metastasis with a continuum-discrete model. International Congress on Technology. IEEE. https://doi.org/10.1109/ictck.2015.7582700

Yin SF, Xue SL, Li B, Feng XQ (2019) Bio-chemo-mechanical modeling of growing biological tissues: finite element method. Int J Non-Linear Mech 108:46–54. https://doi.org/10.1016/j.ijnonlinmec.2018.10.004

Zhang L, Athale CA, Deisboeck TS (2007) Development of a three-dimensional multiscale agent-based tumor model: simulating gene–protein interaction profiles, cell phenotypes and multicellular patterns in brain cancer. J Theor Biol 244:96–107. https://doi.org/10.1016/j.jtbi.2006.06.034

Ziani L, Chouaib S, Thiery J (2018) Alteration of the antitumor immune response by cancer-associated fibroblasts. Front Immunol 9:414. https://doi.org/10.3389/fimmu.2018.00414